IOP Publishing Nanotechnology
Nanotechnology 26 (2015) 395703 (9pp) doi:10.1088/0957-4484/26/39/395703

Electrical properties of ZnO single nanowires

Markus Stiller, José Barzola-Quiquia, Mahsa Zoraghi and Pablo Esquinazi

Division of Magnetism and Superconductivity, University of Leipzig, 04103 Leipzig, Germany

E-mail: markus@mstiller.org

Received 28 May 2015, revised 24 July 2015
Accepted for publication 13 August 2015
Published 11 September 2015

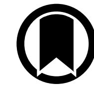

Abstract

We have investigated the electrical resistance $R(T)$ of ZnO nanowires of ≈ 400 nm diameter as a function of temperature, between 30 K and 300 K, and frequency in the range 40 Hz to 30 MHz. The measurements were done on the as-prepared and after low-energy proton implantation at room temperature. The temperature dependence of the resistance of the wire, before proton implantation, can be well described by two processes in parallel. One process is the fluctuation induced tunneling conductance (FITC) and the other the usual thermally activated process. The existence of a tunneling conductance was also observed in the current–voltage ($I-V$) results, and can be well described by the FITC model. Impedance spectroscopy measurements in the as-prepared state and at room temperature, indicate and support the idea of two contributions of these two transport processes in the nanowires. Electron backscatter diffraction confirms the existence of different crystalline regions. After the implantation of H^+ a third thermally activated process is found that can be explained by taking into account the impurity band splitting due to proton implantation.

Keywords: ZnO nanowires, electrical transport, fluctuation induced tunneling conduction, proton implantation

1. Introduction

Zinc oxide (ZnO) nanostructures have recently drawn attention due to a wide potential applicability in electronics and optoelectronics in both theoretical and experimental physics [1–3]. ZnO nanostructures have a large surface/bulk ratio, which makes them in general interesting for optical devices and bare a great potential for nanoscale electronic devices [4, 5]. The huge surface to volume ratio also results in a high influence of adsorbates at the ZnO NW surface on the electrical transport properties [6, 7].

ZnO is a wide band-gap semiconductor with a band gap of 3.4 eV and, in a undoped (native) state it exhibits n-type conduction. The n-type characteristics are believed to originate from native defects (e.g. structural defects or impurities), however the origins of these imperfections and their corresponding impurity levels are still under question [8–11]. The dopant levels are sensitive to the sample preparation and can be categorized into shallow levels (30–60 meV) and deep levels (100–600 meV) [12].

Several electronic transport mechanisms have been reported in the literature, yet many of these works have been performed using the two-probe method [13–16]. Such metal–semiconductor–metal structures are used for electronic nanodevices such as field-effect transistors (FETs) [17, 18–21], sensors [18, 22] or photo-detectors [23, 24]. In such systems, the contact resistances are usually large and temperature dependent [12] and therefore the resistance measurements are influenced by these contributions. Due to such complications, conclusions obtained from such measurements are doubtful.

For instance, variable-range hopping (VRH) has been suggested as the main transport mechnism in ZnO nanowires (NWs) when using the two-probe method [14]. On the other hand, a combination of nearest-neighbor hopping (NNH) and thermal activation has been used and proposed as conduction mechanism in ZnO NWs using the four-probe method [12]. However, we note that the presence of non-ohmic $I-V$ curves are not in agreement with the use of the before mentioned transport mechanism.

In our study we show that the resistance of ZnO nanowires of relatively large diameter follows the (non-ohmic) fluctuation induced tunneling conduction (FITC) model together with a thermal activation process. We have

 © 2015 IOP Publishing Ltd Printed in the UK

investigated the transport properties of ZnO nanowires before and after proton implantation. From our results we not only get information about the dominant transport mechanism in this system, but we also study the influence of implanted protons on the conduction.

2. Experiment

ZnO nanowires were prepared from a high purity initial material (ZnO: 99.99% Merck) in form of powder. ZnO powder and graphite powder (6N, Ringsdorff, Germany) were mixed with equal weights. After that the powder mixture was pressed into pellets with a pressure of $P \approx 5 \times 10^6$ Pa. The NWs were then prepared by the carbothermal process, which involves the thermal decomposition of ZnO [25] at $T \approx 1150$ °C in a tubular furnace placed in the air. Initially, we obtained a bundle of microwires and nanowires. The perimeter of the wires with a diameter $\leqslant 1$ μm is circular, as is the case for the nanowire studied in this work. Using the carbothermal method, the typical hexagonal shape develops only for ZnO wires with diameters larger than $\approx 1 \mu$m. Circular shaped nanowires are already known to exhibit structural defects [26, 27]. A ZnO nanowire and a microwire are shown in figures 1(a) and (b). As can be seen in the figure, the shape of the ≈ 9 μm diameter wire is hexagonal and the ≈ 416 nm wire has a circular perimeter. A bundle of wires was placed between two substrates and when pressure was applied, NWs where transfered onto the top of the silicon substrates (caped with a SiO_2 surface layer) by mechanical and electrostatic forces. Using a scanning electron microscope (Nova NanoLab 200, FEI Company) and electron beam induced deposition (EBID) of amorphous WC_x, the NWs were fixed onto the substrate (see figure 1(b)). The deposited WC_x is nearly insulating [28] and does not only fix the NWs but also helps to prepare the electrical contacts. For that, the substrates were covered with a resist (PMMA 950 K, AR-P 671-05) and electron beam lithography was used to design the structures for the contacts. A bilayer film consisting of Cr (5 nm) and Au (35 nm) was then sputtered onto the substrate-sample-PMMA configuration. After removing the PMMA, the samples were contacted onto a chip carrier for further measurements.

For the transport measurements, the carrier is placed on the cold head of a standard closed cycle refrigerator inside a vacuum bell, with a minimal temperature of $T \approx 30$ K. The electrical resistance was measured in the four probe configuration, using a current source (Keithley 6221) and a nanovoltmeter (Keithley 2182). The results were similar for all electrodes. The results of the temperature dependent resistance as well as the $I{-}V$ curves presented in this paper, have been measured using the contacts in the middle. Due to the configuration of the sample holder and chip carrier, the impedance spectroscopy was measured using a set of contacts shifted by one segment.

The proton/H^+ implantation was done using a self made DC plasma chamber in a parallel plate setup at room temperature with Ar/H (Ar:90%, H:10%, Air Liquide) gas mixture [29]. The chip carrier with the NWs were mounted on a plate placed about 10 cm away from the plasma center. An applied bias voltage of 300 V was used to accelerate the H^+ ions toward the samples. The scanning electron microscope (SEM) pictures did not show any change on the wire's shape or surface after low-energy proton implantation. One contact of the ZnO NW was connected to the ground and the bias current was measured. The sample setup was covered with Teflon, such that only a small window above the NW was opened and the huge contacts (compared to the surface of the nanowire) were shielded. This results in a higher concentrations of ions which actually penetrate the surface of the ZnO NW, rather than flowing through the contacts. The parameters are shown in table 1. We will present the results of an individual nanowire, before and after hydrogen plasma treatment. At this point, we emphasize that we have chosen a nanowire with a diameter such that we have a resistance in the order of few MΩ at room temperature. This allows us to be able to measure at low temperatures and also to avoid the destruction

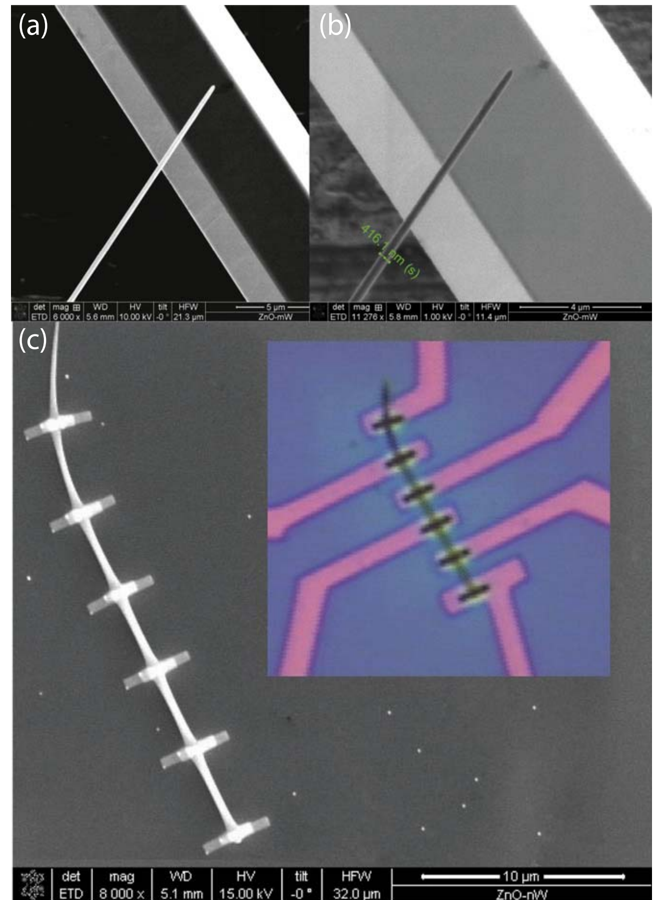

Figure 1. In both figures (a) and (b) the SEM pictures of two ZnO wires are shown, which were grown using the carbothermal method. The scale bars at the bottom right denote 5 μm and 4 μm, respectively. The smaller nanowire with a diameter of ≈ 416 nm has a circular perimeter and is standing at the top of the larger microwire of ≈ 9 μm diameter. In both SEM pictures the hexagonal shape of this microwire can be recognized. In (c) a ZnO nanowire fixed with EBID prepared WC_x structures is shown. The inset shows the NW with Cr/Au contacts.

Table 1. Parameters for the hydrogen plasma implantation used for the ZnO nanowire.

NW	U_{bias} (V)	I_{bias} (μA)	P (mbar)	t (min)
nW1a	300	5	1E-3	90

of the wire during the ion implantation due to the high voltage and current used. The investigated ZnO nanowire has a diameter of $d \approx 401$ nm according to the scanning electron microscope (SEM) measurements. The length between two contacts is $l \approx 5$ μm.

To carry out the impedance spectroscopy an Agilent 4294A precision impedance analyzer was used. The measurements were done at room temperature with a frequency range of 40 Hz–30 MHz.

3. Results

In this section we present and discuss the obtained results. Section 3.1 describes first the as-prepared NW (ZnO-NW-ap) followed by section 3.2 with the presentation and discussion of the NW treated with protons (ZnO-NW-aH). Finally in section 3.3 we present the impedance spectra for the ZnO-NW-ap sample, which confirms the internal grain-like structure of the NW.

3.1. As-prepared ZnO NW.

The resistance as a function of temperature of the ZnO-NW-ap sample is presented in figure 2. We have measured it using different applied currents. We observe, that at temperatures $T < 150$ K, the resistance depends on the applied current. In order to clarify this current dependence, we have performed current–voltage ($I-V$) measurements at different constant temperatures, the results are presented in figure 3. The $I-V$ curves are clearly non-linear at $T < 125$ K. The behavior is close to that of a sample with a barrier, and is usually observed in measurements done using two-point method. However, we have used a conventional four point method, which discards the influence of the contact barrier. That means, the nature of the non-linear behavior in the $I-V$ curves has another source and should be temperature dependent. In order to describe our results with a consistent theory, which is able to predict the behavior in $R(T)$ and in the $I-V$ curves with common parameters, we have used the fluctuation induced tunneling conduction (FITC) model [30]. This model can be used to describe similar behavior observed in similar materials such as oxide nanostructures [31–34], double walled carbon nanotubes bundles [35], conductor-insulator composites [36, 37], disordered semiconductors [38] or doped organic semiconductors [39, 40].

According to the FITC model, at small applied electric fields (where the $I-V$ curves are linear) the temperature dependent electrical resistance across a small junction is

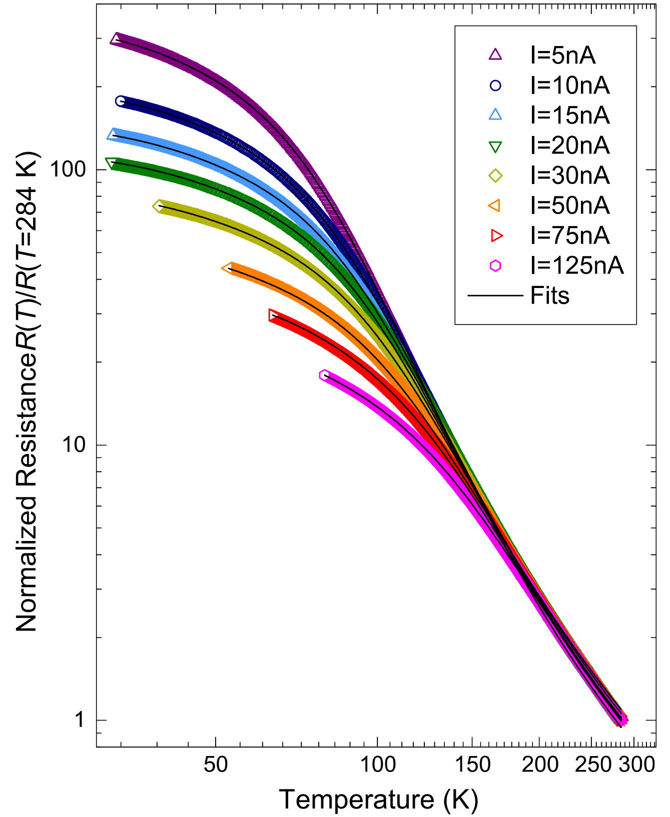

Figure 2. The normalized temperature dependent resistance at different applied currents for the as-prepared ZnO-NW-ap. The lines are the fits.

described by

$$R_{\mathrm{FITC}}(T) = R_\infty \exp\left(\frac{T_1}{T_0 + T}\right), \tag{1}$$

where R_∞ is a parameter which depends only weakly on T and the characteristic temperatures T_1 and T_0 defined as

$$T_1 = \frac{8\varepsilon_r\varepsilon_0}{e^2 k_B}\frac{A\phi_0^2}{w} \quad \text{and} \tag{2}$$

$$T_0 = \frac{16\varepsilon_r\varepsilon_0}{\pi\sqrt{2m}\,k_B e^2}\frac{A\phi_0^{3/2}}{w^2}, \tag{3}$$

where ε_0 is the permittivity of vacuum, ε_r is the dielectric constant of the insulating barrier, e is the elementary charge, k_B the Boltzmann constant, 2π is the Planck's constant, m is the electronic mass, A is the area of the tunnel junction, ϕ_0 is the barrier height and w is the barrier width. The characteristic energy $k_B T_1$ can be regarded as the energy required for an electron to cross the barrier and T_0 is the temperature well below thermal fluctuations become insignificant.

The FITC model also provides a way to analyze the non-linear $I-V$ curves for large applied electric fields at a given temperature:

$$I_{\mathrm{FITC}}(V) = I_s \exp\left[-a(T)\left(1 - \frac{V}{V_s}\right)^2\right], |V| < V_s, \tag{4}$$

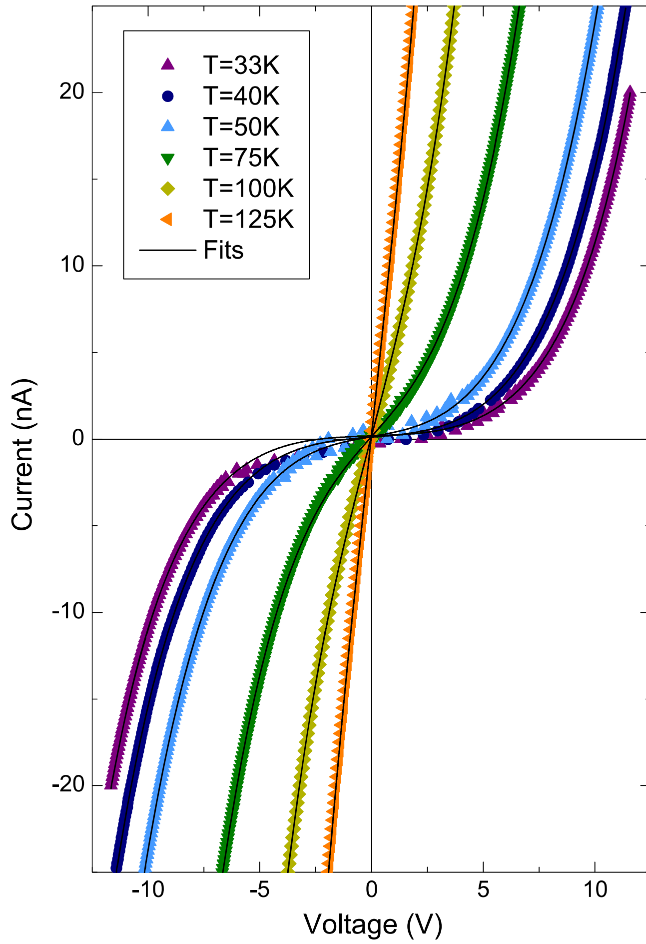

Figure 3. The $I-V$ curves at different constant temperatures for the as prepared ZnO-NW-ap. The curves at $T \geqslant 150$ K are linear (not shown), where the behavior is dominated by thermal activation. The black lines are the fits to equation (8).

where the saturation current I_s and critical voltage V_s depend only weakly on T and $a(T)$ describes the influence of the temperature on the $I-V$ curves:

$$a(T) = \frac{T_1}{T_0 + T}. \tag{5}$$

This implies that the characteristic temperature T_1 and T_0 can be obtained by fitting the results to equation (1) and by fitting $a(T)$ to equation (5), extracted by fitting the $I-V$ curves to equation (4) (with the ohmic regime being excluded) at different temperatures. This allows us for a self consistency check of the model. We also found that at high temperatures, where the $I-V$ results are linear, the resistance obeys the temperature activated transport process, given as:

$$R_a(T) = R_0 \exp\left(\frac{E_a}{k_B T}\right). \tag{6}$$

where E_a is the activation energy and R_0 a free prefactor. In order to describe the complete temperature dependence of the experimental results, we have used a simple model, consisting of three contributions in parallel. One is the before mentioned FITC resistance R_{FITC}, the second one is the temperature

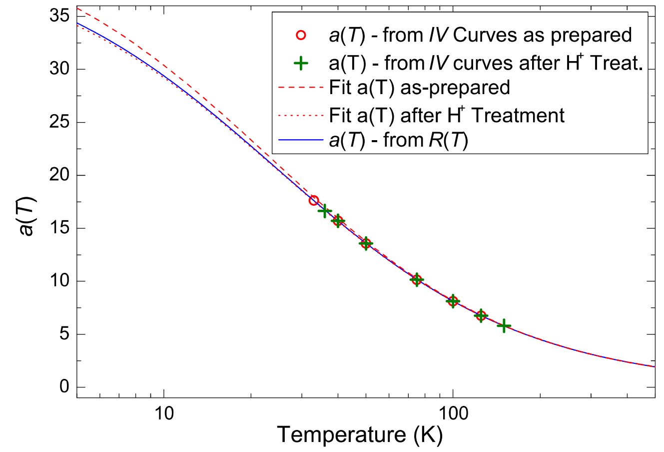

Figure 4. The temperature dependent parameter $a(T)$, obtained from the $I-V$ curves (red circles) and from the temperature dependence of the electrical resistance (blue line) for the as-prepared ZnO-NW-ap. The values obtained from the $I-V$ curves after H^+ treatment (ZnO-NW-aH) are shown as green crosses. The obtained parameters (see table 2): $T_{1,IV}$ and $T_{0,IV}$ are the characteristic temperature T_1 and T_0 (see equations (2) and (3), respectively) obtained from the fits to equation (5) using parameter $a(T)$, which was obtained from the fits of the $I-V$ curves before treatment (see figure 3) and after treatment (see figure 6); $T_{1,R}$ and $T_{0,R}$ are the characteristic temperatures T_1 and T_0 obtained from the fits to equation (1) for both, the as-prepared ZnO-NW-ap and the wire after proton implantation (see figure 5).

activated resistance and finally a temperature independent term R_0. The total resistance R_{Total} is given as follows:

$$R_{\mathrm{Total}}^{-1}(T) = R_{\mathrm{FITC}}^{-1}(T) + R_a^{-1}(T) + R_0^{-1} \tag{7}$$

Using equation (7), we have fitted our data, see figure 2. We observe that our model describes very well the experimental results in the whole temperature range. The value obtained for the activation energy is $E_a = (20.2 \pm 1.2)$ meV, which is in the same range of other ZnO Samples from the literature [25, 41, 42]. This activation energy corresponds to shallow defect levels produced by Zn interstitials, oxygen vacancies and also H^+ in ZnO (according to theoretical calculations [43] and experimental observations by photoluminescence [44]). The presence of H^+ in our sample is a direct consequence of the used method to prepare the nanowires, i.e. during the growth at air, water vapor serves as hydrogen source, which diffuses into the wires [10].

From the fits we obtained also the characteristic temperatures T_1 and T_0, and using equation (5) we calculate the temperature dependence of $a(T)$. The result is plotted in figure 4 (blue line). In figure 4 we can also see the results obtained after hydrogen plasma treatment, which will be discussed in section 3.2. The values obtained from the fits are comparable to other oxide materials [34, 45].

In the next step we have fitted the $I-V$ results using two contributions, one comes from the FITC model and a linear term which contains the contribution of the before mentioned activated term of the resistance and the temperature

independent term. The total $I_{\text{Total}}(V)$ is given by the equation:

$$I_{\text{Total}}(V) = I_{\text{FITC}}(V) + I_a(V), \tag{8}$$

where $I_{\text{FITC}}(V)$ is given by equation (4) and $I_a(V)$ is a linear term. The results using equation (8) are plotted in figure 3 as straight lines. The experimental results are well described by the model.

From the $I_{\text{FITC}}(V)$ we obtain the parameter $a(T)$ at each constant temperature. The obtained values are plotted in figure 4 as (o). These data can be fitted using equation (5) and is plotted in figure 4 as dashed line. From the fit we obtain the characteristic values for $T_{1,IV}$ and $T_{0,IV}$. If we compare the results for $a(T)$ obtained from $R(T)$ and $I-V$, we conclude that our results obtained by both measurements are consistent with each other, indicating that the transport mechanism at low temperatures is preferentially well described and dominated by the FITC transport process.

We would like to remark on the parameters we get from the fitting procedure. The relative high number of parameters can cause artifacts, which is a common problem when the transport properties depend on 3 or more different processes. Therefore, a summary of how the parameters were obtained will be given. The first step was the fitting of the $I-V$ curves of the as-prepared nanowires, see figure 3. Within in the fitting procedure the following restrictions have been made: the critical voltage V_c and the saturation current I_s depend only weakly on the temperature; also the applied voltage must satisfy $|V| < V_c$. In this way we obtained initial results for $a(T)$. These values were cross-checked with the resistance measurements of the as-prepared wire until good agreement between the $I-V$ curves and $R(T)$ was found. In order to check for the consistency of the obtained parameters, the resistance measurements before and after treatment were then taken into account. In this fitting procedure, the parameters, which do not depend on proton implantation, were taken as shared parameters, i.e the curves were fitted simultaneously with the critical temperatures T_1, T_0 and the activation energy for the bulk E_a as global parameters for all curves. The $I-V$ curves for the treated nanowire, see figure 6, were fitted in the same way as in the as-prepared case and included in the procedure. Finally, the consistency of all obtained parameters was verified (see figure 4), i.e. the results of the $I-V$ curves should agree with the results obtained from the resistance measurements (in the as-prepared case and after H^+ treatment). The fitting yields values of I_s between 0.05 A and 0.5 A, and the values of V_c lie between 115 V and 120 V. The procedure is lengthy but necessary in order to get reliable results. In general, it is possible to fit either a $I-V$ curve or a temperature dependent measurement with quite different parameters. However, one gets contradictions with parameters obtained from other measurements, and/or values which do not make physical sense, such as negative values, large changes of V_s or values for T_1 and T_0 which do not follow equation (5). The sharing of the parameters between the as-prepared and implanted states of the sample is a great help and reduces effectively the amount of free parameters.

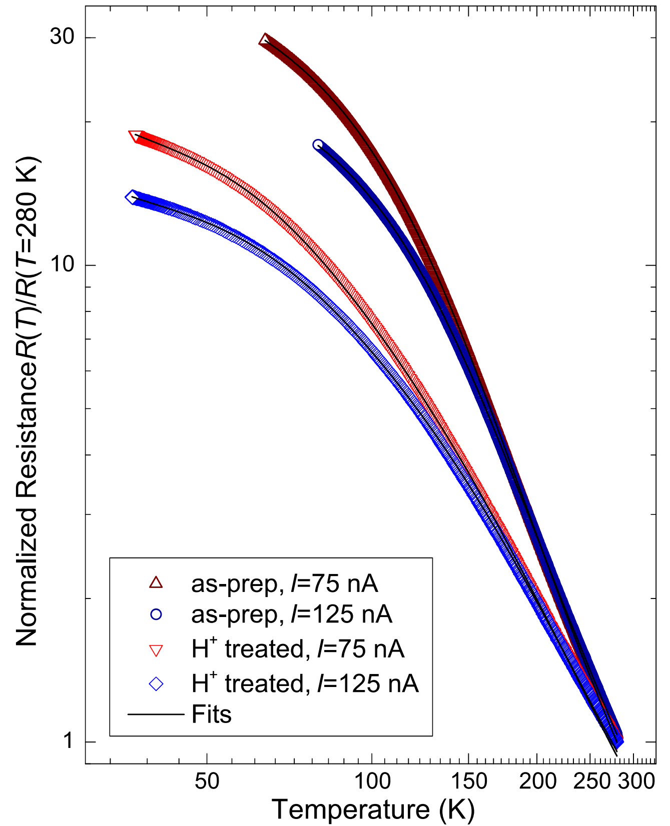

Figure 5. The temperature dependence of the electrical resistance at different applied currents for the ZnO NW before and after H^+ implantation. The black lines are the fits using equation (7) (as-prepared NW) and equation (9) (after proton implantation), the characteristic temperatures $T_{1,R}$ and $T_{0,R}$ have been taken as shared parameters.

3.2. Proton implanted ZnO NW

In a second step, we have implanted H^+ in our ZnO NW by the method described before. In order to have some information about the modified region, such as penetration depth, defect density, etc. we have performed calculations using Monte Carlo simulations provided by the stopping range of ions in matter (SRIM) program [46]. We calculated the penetration depth of the H^+ according to our experimental conditions (see inset figure 6). The estimated penetration length is $d \approx 10$ nm, indicating that only ≈4.8% of the total volume of the sample is modified and the main changes occur close to the surface. After hydrogenation, the resistance decreases, which is in agreement with results from literature [29, 47, 48]. We have repeated our measurements in the same way as for the as-prepared sample. The resistance measurements of the treated, as well as the as-prepared results, are plotted in figure 5 together with the fits obtained using equation (7) for the corresponding applied currents. Similar as in the case of the untreated samples, the model describes well our results. We added a thermally activated contribution R_{H^+}, which will describe the electrical transport in the modified part in the nanowire due to the H^+ implantation:

$$R(T)^{-1}_{\text{Total}} = R(T)^{-1}_{\text{FITC}} + R(T)^{-1}_{A} + R_0^{-1} + R^{-1}_{H^+} \tag{9}$$

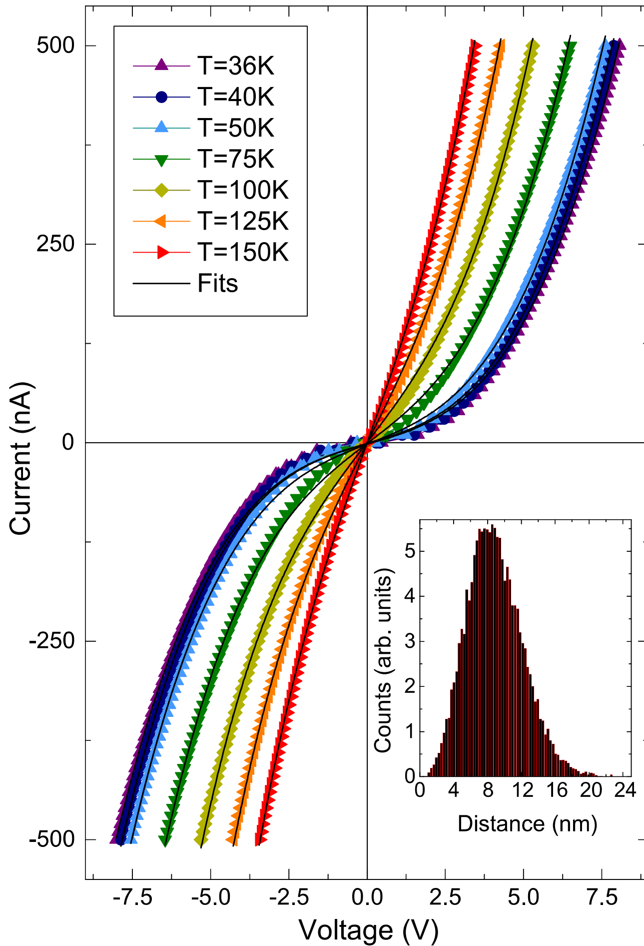

Figure 6. The $I-V$ curves at different constant temperatures for the ZnO NW after H^+ implantation. The red lines are the fits using the FITC model. The inset shows the SRIM results and yield a penetration depth for H^+ at 300 eV of $d \approx 10$ nm.

The obtained activation energy for the non-modified part remains unchanged, $E_a = (21.5 \pm 0.5)$ meV, within experimental error, because it reflects the behavior of the untreated part of the ZnO NW. For the modified part we obtain $E_{a,H^+} = (1.4 \pm 0.5)$ meV, which is smaller than the result obtained from the non-treated part. This indicates that the resistivity of the hydrogen-treated part of the sample is reduced. The decrease due to the influence of H^+ implantation was already reported in the literature [47].

Also the FITC contribution should not change upon H^+ implantation. Therefore, the resistance of the treated NW was fitted together with the as-prepared results and the characteristic temperatures $T_{1,R}$ and $T_{0,R}$ have been taken as shared-parameters.

We have also measured the $I-V$ curves at different constant temperatures and the results are plotted together with the fits obtained using equation (8) in figure 6. Comparing the values for $a(T)$ obtained from the fitting process of the resistance and the $I-V$ curves, we observe that the parameters $T_{1,IV}$, $T_{0,IV}$ (see table 2 and figure 4) coincide within the experimental error with those of the untreated part. Independently of the fitting process and the transport mechanisms describing our results, an experimental fact is the reduction of the resistance after the H^+ implantation in the ZnO nanowire. A detailed overview of the parameters can be found in tables 2 and 3.

In order to calculate the change in the resistivity originated by the H^+ in the shell of our ZnO NW, we assumed that the total resistance measured after the treatment behaves like a parallel resistance—one contribution is due to the H^+ treated part (with a resistivity ρ_{H^+}) and the other one is the unmodified core of the wire (ρ_{core} with a diameter of 391 nm). The calculated values are shown in table 3. The resistivity $\rho_0 \equiv \rho_{core}$ for pure ZnO is in agreement with literature values [49], and, as expected, we obtained a reduction of one order of magnitude for the H^+ treated part. Changes up to four orders of magnitude in the resistivity were already observed in nanorods and nanowires, respectively, when they were exposed to a moisture pulse of 97% relative humidity, where water will be dissociated and provides protons as charge carriers for the transport [50]. Such resistivity values are comparable to semi-metal materials such as BiSb [51] and high doped Si with phosphorus or boron as dopants (doping density $d_{P,B} \approx 10^{16}\,cm^{-3}$) [52]. According to our experimental parameters and the SRIM calculations we obtain a similar implantation density of $d_{H^+} \approx 10^{16}\,cm^{-3}$.

According to theoretical calculations done for c-axis oriented ZnO nanowires [53], it was predicted that the absorption of H can reduce the resistivity and moreover induce a metal-like behaviour when each H provides one electron to the modified part of the nanowire. There are also some experimental results showing the reduction of the resistivity in bulk and in thin films after H^+ treatment, where a metallic like regime was reported at high temperatures [29, 47].

Due to the high energy gap of 3.4 eV of ZnO, the excitation of carriers to the conduction band will not occur at the measured temperatures. However, it is well known that ZnO NWs are often doped with n-type defects [18, 20, 21], where the impurity levels of shallow defects are 30–60 meV below the conduction band. The doping levels can be categorized into low, moderate and high doping. Low doping leads to hopping conduction of electrons to localized site, high doping the forming of an impurity band, where the conduction is metallic like and independent of temperature. Moderate doping ($\approx 6 \cdot 10^{16}\,cm^{-3}$), which is described by the overlapping of the wave functions [54], results in an activated conduction. Our H^+ implantation yields a moderate to high doping. The Coulomb fields from the acceptors and ionized donors will cause the donor levels to split into an impurity band [55], which again splits into the lower D band (formed by single charged donors, Fermi level lies within the D band for moderately doped ZnO NWs) and upper D^- band (formed by neutral donors) [54, 56, 57]. When the impurity concentration is high enough (but not so high that metallic conduction sets in) the two impurity bands and the bottom of the conduction band smear over and the etch states of two neighboring bands form localized states. This implies, that due to $k_B T$ the electrons might be excited to the upper D^- band, with a larger donor orbital and wave function compared

Table 2. The characteristic temperatures $T_{1,R}$, $T_{0,R}$ (shared parameters) obtained by fitting $R(T)$, $T_{1,IV}$, $T_{0,IV}$ obtained using the $I-V$ curves, the activation energy E_a before and after hydrogen plasma treatment as well as E_{a,H^+} for modified shell of the nanowire.

State	$T_{1,R}$ (K)	$T_{0,R}$ (K)	$T_{1,IV}$ (K)	$T_{0,IV}$(K)	E_a (meV)	E_{a,H^+} (meV)
as-prep.	1011 ± 15	24 ± 3	1007 ± 3	24 ± 1	20.9 ± 1.5	–
H^+ treated			1012 ± 4	25 ± 1		1.4 ± 0.5

Table 3. The resistivity ρ for the as-prepared nanowire/nanowire core, ρ_{H^+} for shell of the nanowire after H^+ treatment and the resistance at room temperature.

State	ρ_0 (Ωcm)	ρ_{H^+} (Ωcm)	R_{RT} (MΩ)
as-prep.	3.44	–	5.38
H^+ treated		0.29	2.64

to the *D* band resulting in a reduced resistivity. Our reduced resistivity and activation energy of the treated NW shell, $E_{a,\mathrm{H}^+} = 1.4$ meV, agrees with this assumption, as E_{a,H^+} should be about half of the energy gap from the Fermi level to the bottom of D^- band. This value is in agreement with the literature [54].

3.3. Impedance spectroscopy of the as-prepared ZnO NW.

The FITC model is applicable for systems where the electronic transport is due to tunneling between large, conducting grains via small contacts or thin barriers, i.e. the sample should have a granular-like structure. A direct evidence of this kind of internal structure in our NW is given in section 3.4. It is known that in nanowires lattice defects, such as stacking faults, can be found, especially in NWs, which have a circular shape [26, 27]. These stacking faults are highly resistive and may explain the observed FITC contribution to the overall conductance.

A simple way to gain some information about the involved conduction mechanisms, is through the use of an indirect method, the complex impedance spectroscopy, which is a very well established method to investigate the transport mechanism in materials containing grains and interface contributions. In figure 7 we present the experimental data (Cole-Cole plot) at room temperature and in darkness in order to avoid influence of natural light containing an UV component [58]. We can recognize that the main arc is composed of three semi circles, indicating that the conduction mechanism in the nanowire consists of three capacitances. In order to get information about the contributions, we propose a simple circuit model to describe the experimental data. The Cole-Cole data can be fitted using a capacitor and a resistance in series (C_2 and R_2) and a capacitance (C_1) in parallel (see inset in figure 7). R_1 takes into the account the long range, frequency independent conductivity. The values are presented in table 4. According to literature, the values obtained for the capacitances can be related to different mechanisms of electrical conduction and contributions [59]. In our case, we obtained for $C_1 = 1.8 \times 10^{-11}$ F, which corresponds to grain boundaries and C_2, being one order of magnitude smaller, is

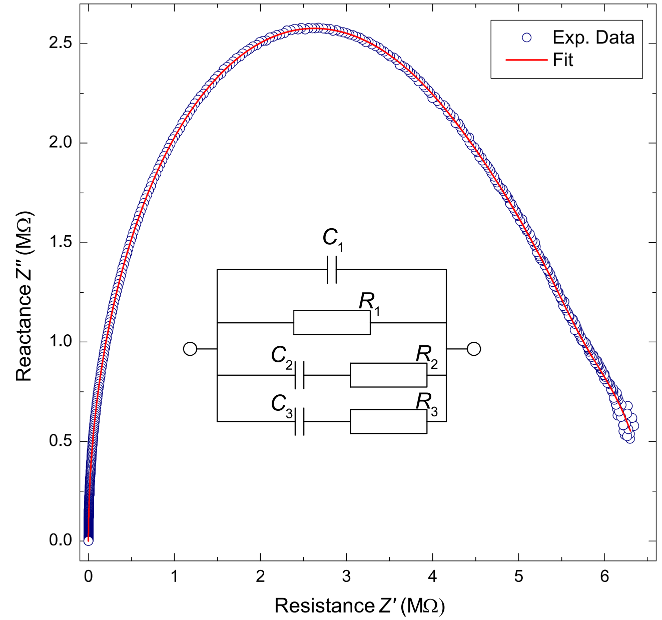

Figure 7. The reactance versus resistance for the as-prepared ZnO NW. The line is the fit using the shown model.

Table 4. The parameters obtained by fitting the impedance spectra using the model shown in the inset in figure 7.

C_1 (pF)	R_1 (MΩ)	C_2 (pF)	R_2 (MΩ)	C_3 (pF)	R_3 (MΩ)
18.2	6.5	8.3	42	35.6	55

the average capacitance at the points of closet approach—where the main fluctuation induced tunneling occurs—and therefore, can be seen as part of C_1. R_2 is the resistance across the junction. A third contribution, consisting of a capacitor and a resistor, had to be added in order to fit the complete arc. We attribute these to a second tunneling process across the grain boundaries which have a larger area and capacitance, note that the charging energy $e^2/2C_3$ is negligible [30] for DC measurements. The fact, that we can observe this kind of behavior in our ZnO nanowire already at room temperature is important, because it supports the idea of conducting regions, which are separated by small barriers. We expect, that the three arcs in Cole-Cole plot become even more evident for temperatures well below room temperature.

3.4. Electron backscatter diffraction

According to the transport measurements (FITC model and impedance spectroscopy) our ZnO NW is composed of different crystalline regions, i.e. it is not a single crystal. In order

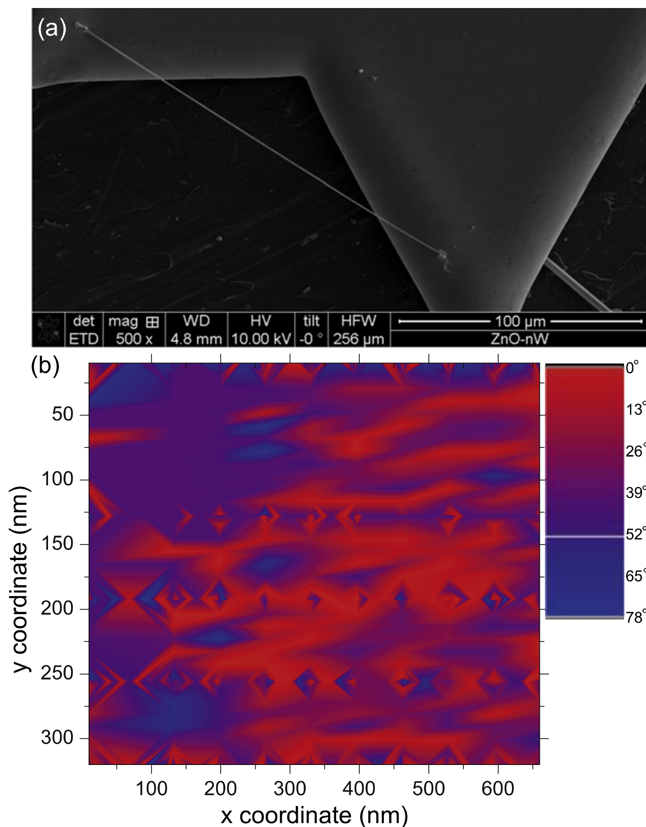

Figure 8. (a) shows the ZnO NW fixed on both ends to the sample holder. EBID of platinum was used to attach the wire. In (b) the results of EBSD measurements are shown for a scanned area of (660×320) nm. Taking the main axis of the wire as reference (x-axis in the figure), the colors show the deviation of the c-axis from this vector, with a maximum of 78°.

to get direct information about the granular like structure, we have performed electron backscatter diffraction (EBSD) experiments. Using this microstructural-crystallographic technique we directly obtain information about the crystallographic orientations within the sample, i.e. about possible texture or preferred grain orientations.

For this experiment we used a ZnO NW separated of the same bundle used for the former nanowire and with similar diameter (≈600 nm) and cylindrical shape. Using EBID with PtC_x, the NW was fixed to a V-shaped sample holder, which can be seen in figure 8(a). Using an ion beam, the wire was thinned such that we can measure across the wire and also get extensive data in a large region in the order of the diameter of the nanowire. Measurements have been performed in different regions giving similar results.

In figure 8(b) the deviation of the c-axis from the main direction of the NW is shown, i.e. 0° corresponds to the 001 direction parallel to the main axis of the wire and 90° would be the maximal possible deviation (rotations around the c-axis are not included in the figure). According to the results, large fractions of the wire grow with a deviation up to ≈ 30°. There are some regions of the NW with a deviation up to ≈ 78°, crystal orientations with a higher angle away from the main axis were not found. This shows that our ZnO NW is not a perfect single crystal, but rather consists of several crystalline regions with different orientations. The results confirm the granular like structure of the NW. From EBSD we can get a rough estimate of the cross-sectional area of the grains and find $A_g \approx (100\ \text{nm} \times 50\ \text{nm})$.

Fluctuation induced tunneling can occur at the interfaces between these regions, while an activated conduction mechanism is present within these domains. These results are in agreement with the observed impedance spectroscopy and support the idea of grains present in the nanowire. Dividing the characteristic temperatures, T_1/T_0, and assuming a barrier width of $w = 10$ nm, we can estimate the barrier height and area of the points of closest approach, where the fluctuation induced tunneling occurs (this is not the area of the grains). We assume a relative large barrier thickness due to the presence of lattice defects, which act as electronic traps and the resulting formation of a depletion layer which acts as a barrier. In this way we find a barrier height of $\phi_0 \approx 274$ meV and an area of $A \approx (60\ \text{Å})^2$. This value of A is compatible with the expectations of the FITC model, that assumes an area several orders of magnitude smaller than the total surface area of the grains.

4. Conclusion

We have measured the transport properties of a ZnO nanowire in a conventional four point method. The as-prepared sample was investigated as well as after the implantation of H^+. Using the FITC model and an energy activated term, we were able to describe the full temperature dependence of the resistance and also the current-voltage characteristic curves. Impedance results indicate that the ZnO nanowire has mainly two different contributions in the conductivity. EBSD shows that our ZnO NW is not a single crystal, but it is composed of crystalline regions having different orientations. This is compatible with the impedance spectroscopy results and supports the application of the FITC model. According to our results, the density of H^+ implanted produced a large change in the resistivity of the irradiated region and introduced a third conduction mechanism. This provides the possibility of tailoring the transport properties of single ZnO nanowires through modifying the surface by means of a controlled implantation of H^+.

Acknowledgments

This work has been supported by the Collaborative Research Center SFB ∼ 762 ‘Functionality of Oxide Interfaces’.

References

[1] Pearton S, Norton D, Ip K, Heo Y and Steiner T 2003 *Superlattices Microstruct.* 34 3–32

[2] Özgür Ü, Alivov Y, Liu C, Teke A, Reshchikov M, Doğăn S, Avrutin V, Cho S J and Morkoç H 2005 *J. Appl. Phys.* 98 041301
[3] Klingshirn C 2007 *Basic Solid State Phys.* 244 3027–73
[4] Kong Y, Yu D, Zhang B, Fang W and Feng S 2001 *Appl. Phys. Lett.* 78 407
[5] Yao B, Chan Y and Wang N 2002 *Appl. Phys. Lett.* 81 757
[6] Liao Z M, Liu K J, Zhang J M and X J Yu D P 2007 *Phys. Lett.* A 367 207–10
[7] Liao Z M, Lv Z K, Zhou Y B, Xu J, Zhang J M and Yu D P 2008 *Nanotechnology* 19 335204
[8] Lany S and Zunger A 2007 *Phys. Rev. Lett.* 98 045501
[9] Hofmann D, Hofstaetter A, Leiter F, Zhou H, Henecker F and Meyer B 2002 *Phys. Rev. Lett.* 88 045504
[10] de Walle C G V 2000 *Phys. Rev. Lett.* 85 1012–5
[11] Look D, Farlow G, Reunchan P, Limpijumnong S, Zhang S and Nordlund K 2005 *Phys. Rev. Lett.* 95 225502
[12] Chiu S P, Lin Y H and Lin J J 2009 *Nanotechnology* 20 015203
[13] Schlenker E, Bakin A, Weimann T, Hinze P, Weber D, Gölzhäuser A, Wehmann H H and Waag A 2008 *Nanotechnology* 19 365707
[14] Ma Y J, Zhang Z, Zhou F, Lu L, Jin A and Gu C 2005 *Nanotechnology* 16 746–9
[15] Lin X, He X, Yang T, Guo W, Shi D, Gao H J, Ma D, Lee S, Liu F and Xie X 2006 *Appl. Phys. Lett.* 89 043103
[16] Heo Y, Tien L, Norton D, Kang B, Ren F, Gila B and Pearton S 2004 *Appl. Phys. Lett.* 85 2002–4
[17] Heo Y, Tien L, Kwon Y, Norton D, Pearton S, Kang B and Ren F 2004 *Appl. Phys. Lett.* 85 2274
[18] Fan Z, Wang D, Chang P C, Tseng W Y and Lu J 2004 *Appl. Phys. Lett.* 85 5923
[19] Song S, Hong W K, Kwon S S and Lee T 2008 *Appl. Phys. Lett.* 92 263109
[20] Chang P C, Chien C J, Stichtenoth D, Ronning C and Lu J 2007 *Appl. Phys. Lett.* 90 113101
[21] Goldberger J, Sirbuly D, Law M and Yang P 2004 *Physi. Chem.* B 109 9–14
[22] Law J and Thong J 2008 *Nanotechnology* 19 205502
[23] Liao Z M, Xu J, Zhang J M and Yu D P 2008 *Appl. Phys. Lett.* 93 023111
[24] Jin Y, Wang J, Sun B, Blakesley J and Greenham N 2008 *Nano Lett.* 8 1649–53
[25] Villafuerte M, Ferreyra J, Zapata C, Barzola-Quiquia J, Iikawa F, Esquinazi P, Heluani S, de Lima M Jr and Cantarero A 2014 *J. Appl. Phys.* 115 133101
[26] Wu Z, Chen I, Lin Y, Chiu S, Chen F, Kai J, Lin J and Jian W 2008 *New J. Phys.* 10 033017
[27] Levin I, Davydov A, Nikoobakht B, Sanford N and Mogilevsky P 2005 *Appl. Phys. Lett.* 87 103110
[28] Spoddig D, Schindler K, Rödiger P, Barzola-Quiquia J, Fritsch K, Mulders H and Esquinazi P 2007 *Nanotechnology* 18 495202
[29] Khalid M and Esquinazi P 2012 *Phys. Rev.* B 85 134424
[30] Sheng P 1980 *Phys. Rev.* B 21 2180
[31] Filipi C, Levstik A, Kutnjak Z, Umek P and Aron D 2007 *J. Appl. Phys.* 101 084308
[32] Konezny S, Richter C, R S III, Parent A, Brudvig G, Schmuttenmaer C and Batista V 2011 *Phys. Chem. Lett.* 2 1931–6
[33] Lin Y H, Chiu S P and Lin J J 2008 *Nanotechnology* 19 365201
[34] Lin Y H and Lin J J 2011 *J. Appl. Phys.* 110 064318
[35] Barzola-Quiquia J, Esquinazi P, Lindel M, Spemann D, Muallem M and Nessim G 2015 *Carbon* 88 16–25
[36] Sheng P, Sichel E and Gittleman J 1978 *Phys. Rev. Lett.* 40 1197–200
[37] Sichel E, Gittleman J and Sheng P 1978 *Phys. Rev.* B 18 5712
[38] Redfield D 1975 *Adv. Phys.* 24 463–87
[39] Chiang C, Fincher C F Jr, Park Y, Heeger A, Shirakawa H, Louis E, Gau S and MacDiarmid A 1978 *Phys. Rev. Lett.* 40 1472
[40] Seeger K, Gill W, Clarke T and Street G 1978 *Solid State Commun.* 28 873–8
[41] Chang P C and Lu J 2008 *Appl. Phys. Lett.* 92 212113
[42] Heo Y, Norton D, Tien L, Kwon Y, Kang B, Ren F, Pearton S and LaRoche J 2004 *Mater. Sci. Eng.* R47 1–47
[43] Look D, Reynolds D, Sizelove J, Jones R, Litton C, Cantwe11 G and Harsch W 1998 *Solid State Commun.* 105 399–401
[44] Meyer B, Sann J, Hofmann D, Neumann C and Zeuner A 2005 *Semicond. Sci. Technol.* 20 62–66
[45] Lai Y R, Yu K F, Lin Y H, Wu J C and Lin J J 2012 *AIP Adv.* 2 032155
[46] Ziegler J 2013 *The Stopping and Range of Ions in Matter* (*SRIM-2013*) www.srim.org
[47] Lorite I, Esquinazi P, Zapata C and Heluani S 2013 *J. Mater. Res.* 29 78–83
[48] Lorite I, Wasik J, Michalsky T, Schmidt-Grund R and Esquinazi P 2014 *Thin Solids Films* 556 18–22
[49] Ellmer K 2001 *J. Phys. D: Appl. Phys.* 34 3097–108
[50] Zhang Y, Yu K, Jiang D, Zhu Z, Geng H and Luo L 2005 *Appl. Surf. Sci.* 242 212–7
[51] Red'ko N, Kagan V and Volkov M 2010 *J. Exp. Theor. Phys.* 111 241–5
[52] Hull R 1999 *Properties of Crystalline Silicon* (London: INSPEC)
[53] Xu H, Fan W, Rosa A, Zhang R and Frauenheim T 2009 *Phys. Rev.* B 79 073402
[54] Nishimura H 1965 *Phys. Rev.* 138 815–21
[55] Hung C and Gliessman J 1954 *Phys. Rev.* 96 1226–36
[56] Shklovskii B and Efros A 1984 *Electronic Properties of Doped Semiconductors* (New York: Springer)
[57] Mott N and Davis E 1979 *Electronic Processes in Non-Crystalline Materials* (Oxford: Clarendon)
[58] Dusari S, Barzola-Quiquia J, Esquinazi P and Heluani S 2010 *Solid State Commun.* 150 22–26
[59] Chinarro E, Jurado J, Figueiredo F and Frade J 2003 *Solid State Ion.* 160 161–8